Seeing Double: Coupling between Substrate Image Charges and Collective Plasmon Modes in Self-Assembled Nanoparticle Superstructures

Pattanawit Swanglap,[†] Liane S. Slaughter,[†] Wei-Shun Chang,[†] Britain Willingham,[†] Bishnu P. Khanal,[†] Eugene R. Zubarev,[†] and Stephan Link[†,‡,*]

[†]Department of Chemistry and [‡]Department of Electrical and Computer Engineering, Laboratory for Nanophotonics, Rice University, Houston, Texas 77005, United States

ABSTRACT The interaction between adjacent metal nanoparticles within an assembly induces interesting collective plasmonic properties. Using dark-field imaging of plasmon scattering, we investigated rings of gold nanoparticles and observed that the images were dependent on the substrate. In particular, for nanoparticles assembled on carbon and gold substrates, intensity line sections perpendicular to the ring revealed a significant broadening beyond the optical resolution accompanied by an intensity dip in the middle of the line profile. Overall, this appeared in the image as a "splitting" into two offset circles along the direction of the scattered light polarization. This effect was not observed for a substrate with a low permittivity, such as glass. By varying the substrate as well as selecting different detected wavelengths and polarization components of the excitation light, we were able to confirm that the observed effect was due to coupling of collective plasmon modes with their induced image charges in the supporting substrates. These results suggest that plasmon scattering in extended nanostructures can be spatially modulated by tuning the permittivity of the substrate.

KEYWORDS: gold nanoparticles · surface plasmon resonance · plasmon coupling · substrate effects · dark-field scattering

The localized surface plasmon resonance of metallic nanoparticles (NPs) displays a dramatic dependence on the NP size and shape as well as the surrounding environment.[1−6] The latter property is actively exploited in NP-based surface plasmon resonance sensing.[7−11] For many practical sensing applications, the effect of the substrate on which the NPs reside is of particular interest. In general, the sensitivity of supported NPs is smaller due to the reduction of the area that is available for analyte sensing. To a first approximation, the sensitivity of the localized surface plasmon resonance is proportional to the fraction of exposed NP surface area, and the shift in the surface plasmon resonance can be modeled as a weighted average between the dielectric constants of the substrate and the immersed medium, as verified by ensemble as well as single particle spectroscopy.[12−15]

Considering only an average medium dielectric effect on the surface plasmon resonance for supported NPs is, however, in some cases an oversimplification of the actual optical response. In fact, it is well-known from classical calculations that the electric dipole of an excited molecule or atom placed in the vicinity of a substrate couples to its own partially reflected electric field, resulting in a frequency shift of the emitted radiation.[16,17] A general solution for the scattering of a sphere on a substrate has been obtained by separating the coupled system into the scattering by a sphere in a homogeneous medium, described by Mie theory, and the reflection of radiation by a surface.[18,19] Mirror image multipoles induced in the substrate have also been taken into account in the calculations, and their importance has later been verified experimentally for latex and copper spheres on silicon wafers.[20]

More recent calculations for plasmonic NPs near metallic surfaces have shown that the localized NP surface plasmons couple strongly not only with image multipoles but also with surface plasmon modes of the metallic film.[21−23] Hybridization between localized surface plasmons of the NP and delocalized surface plasmons of the film leads to spectral shifts that depend on the NP−film separation and the film thickness.[21,22,24] Experimentally, a shift toward lower energies has indeed been observed for the surface plasmon resonance of silver and gold NPs on gold films as a function of film thickness, NP size, and NP−film separation, which were on the order of a few tens of nanometers and

* Address correspondence to slink@rice.edu.

Received for review March 14, 2011 and accepted May 11, 2011.

Published online May 11, 2011
10.1021/nn2009694

controlled by dielectric spacers.[24−28] In all cases, this interaction is strongest for p-polarized incident light. Furthermore, large field enhancements have been predicted for the gaps of the NP−film system[22] and observed experimentally by surface-enhanced Raman scattering.[29−32] In addition to near-field coupling for the NP−film system, the importance of image charges has also been shown by far-field interference of light scattered by a NP and its mirror image, where a single gold NP interacted with an aluminum-coated optical fiber mounted to an atomic force microscope cantilever for precise control over gap distances that exceeded 10 μm.[33]

Interestingly, dielectric substrates can also significantly alter the surface plasmon resonance of supported NPs despite the absence of film surface plasmons. For silver nanocubes, the presence of different dielectric substrates caused a second localized surface plasmon resonance to appear at higher energies in the scattering spectrum, which was assigned to a quadrupolar plasmon mode.[9,34] For spherical NPs as well as nanoshells, the presence of the substrate lifts the degeneracy of the dipole mode and its component orientated perpendicular to the substrate shifts to lower energies for p-polarized excitation light. This trend is similar to the one observed for plasmonic NPs interacting with metallic films[29,35,36] and also depends on the NP−film gap, but the amount of red shift is reduced for dielectric substrates.[29] The interaction strength as measured by the shift in the plasmon resonance maximum increases with the permittivity of the substrate.[35,37] In addition, higher order plasmon modes can appear in the optical spectrum of NPs supported on dielectric substrates because of an intraparticle hybridization of NP plasmons whose degeneracy has been lifted due to symmetry breaking by the substrate.[35,37] Because of the absence of film surface plasmons for dielectric substrates, these effects are mediated by induced image charges.[37]

In addition to the discussed spectral changes for a plasmonic NP brought into the vicinity of a metallic or dielectric film, it has been noted that the elastic and inelastic scattering from individual silver and gold NPs appears as doughnut-shaped patterns in the images.[25,26,29,38] This behavior is indicative of a dipole emitter that is orientated perpendicular to the substrate[39−41] and is consistent with a stronger interaction of the NPs with the substrate for out-of-plane polarized light. When the NP−film interaction strength is decreased by changing the film material or NP−film gap, the usual Gaussian intensity point spread function is obtained, illustrating how the direction and polarization of the light scattered by a plasmonic NP can be tuned.[25,26,29,38] Beyond the NP−film system, such control is of great current interest in nanophotonics.[42−45] However, while most studies of NP−film interactions have focused on spectral shifts,[9,21−29,34−37,46−49] only a few reports exist on the scattering patterns of individual NPs.[25,26,29,38] In addition, to the best of our knowledge, no studies have been carried out on the scattering images of assembled NPs interacting with different substrates. For closely spaced NPs, interparticle plasmon coupling becomes important and changes the optical response.[46,50−58] The question therefore arises as to how the scattering pattern for closely spaced plasmonic NPs depends on the nature of the substrate on which the NPs are assembled.

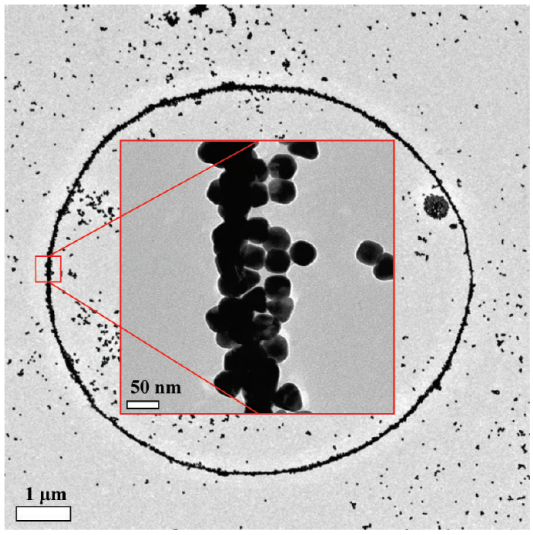

Figure 1. TEM image of a self-assembled gold NP ring on an amorphous carbon layer on top of a copper grid. The ring was composed of 40 nm gold NPs and was 6.8 μm in diameter. The inset shows a magnified TEM image of the ring segment marked by the red box, which illustrates that the width of the self-assembled gold NP ring was several NPs wide.

In this paper, we investigated the effect of coupling between collective plasmon modes of a self-assembled NP ring[58,59] with the substrate on the far-field scattering pattern. Using polarization sensitive and wavelength selective dark-field scattering microscopy, we observed that the images of NP rings appeared as two offset circles displaced from the physical location of the ring for carbon and gold substrates. By varying the substrate material, we show that this effect was due to the interaction between the collective surface plasmon modes of the self-assembled structure and the substrate as the double ring pattern was visible in the images of the NP rings created on carbon and gold but not glass substrates.

RESULTS AND DISCUSSION

Large rings (4−7 μm) of 40 nm gold NPs on different substrates were formed by breath figure templating.[59] A transmission electron microscope (TEM) image of a ring on a 20 nm thick carbon film is shown in Figure 1. The inset is a magnified TEM image of a ring segment which illustrates that the ring was several NPs wide. NP rings were also prepared on glass and gold substrates. The corresponding scanning electron microscope (SEM) images are given in Figure S1 of the Supporting

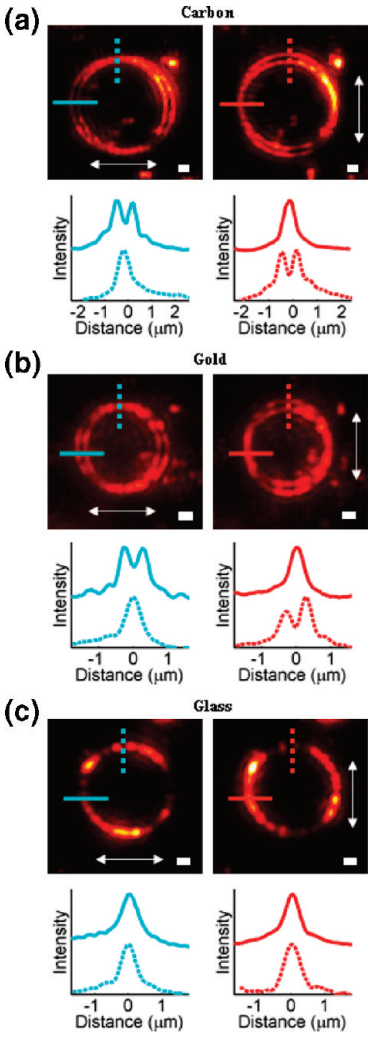

Figure 2. Dark-field scattering images of self-assembled gold NP rings on different substrates: (a) carbon, (b) gold, and (c) glass. The images were collected with a polarizing beam splitter, where the two orthogonal polarization components of the scattered light are indicated by the white arrows. All scale bars correspond to 1 μm. The images were corrected for background scattering, and the intensity scale ranges from 0 to 400 kHz for carbon and from 0 to 200 kHz for gold and glass. Intensity line sections of the ring segments that are indicated by the blue and red lines are given below the corresponding images. The sign of the *x*-axis indicates the position relative to the ring: negative values correspond to positions outside the ring and positive values to positions inside the ring. The intensity line sections were normalized and offset for better comparison.

Information. We previously studied the plasmon scattering of these NP rings using dark-field spectroscopy and found strong interparticle near-field coupling giving rise to collective plasmon resonances polarized along the ring circumference.[58] The scattering spectrum showed several red-shifted plasmon modes that were assigned to multipolar resonances of local ring segments.

The plasmon scattering images of the self-assembled NP rings were strongly influenced by the substrate that the assemblies were created on (Figure 2). Surface plasmon resonances of NP rings on carbon, gold, and glass were excited with randomly polarized light in a dark-field illumination geometry, and the back-scattered light was spectrally integrated (~450−700 nm) and analyzed for two perpendicular polarizations as indicated by the white arrows in Figure 2. For carbon (2a) and gold (2b) as substrates, the polarized dark-field scattering images of the rings appeared as two circles that were offset from each other in the direction of the detected light polarization. However, for the ring on the glass substrate (2c), this effect was not observed. Instead, Figure 2c shows dark-field scattering images of the NP ring consistent with the limited resolution of an optical microscope. The observed effect for the carbon and gold substrates was very reproducible as confirmed by multiple independent measurements of the same and different NP rings. The series of images in Figure S2 taken as a function of microscope focus position furthermore verifies that a misalignment of the optical setup can be ruled out as a possible explanation. It should be noted that the scattering intensities for ring segments aligned parallel to the detected polarization were larger. This is particularly pronounced for the glass substrate and is due to near-field coupling between the NPs leading to longitudinally polarized collective plasmon modes.[58] Variations in scattering intensity along the ring circumference are also influenced by differences in the thickness of local ring segments. The corresponding TEM and SEM images for the rings shown in Figure 2 are given in Figure 1 for the carbon substrate and Figure S1 (Supporting Information) for the gold and glass surfaces, respectively.

The observed "splitting" into offset rings was further analyzed by determining intensity line sections for each polarization component and for different ring segments that were parallel and perpendicular to the detected scattered light as indicated by the red and blue lines in the images shown in Figure 2. The corresponding line sections give the spectrally integrated scattering intensities, as analyzed from the images, and are shown below each image for the three substrates. The origin of the *x*-axis of the intensity line section refers to the position of the ring, while negative values indicate positions in the image outside of the ring and positive values represent positions inside the ring. For the carbon (2a) and gold (2b) substrates, we observed a broadening of the intensity line sections beyond the optical resolution accompanied by a dip in the middle of the line profile for directions that were parallel to the scattered light polarization. This broadening corresponds to the splitting into separated offset rings in the dark-field scattering images. In contrast, the images in Figure 2c for a NP ring on glass did not show the same effect.

In order to quantify the broadening of the intensity line sections, we calculated their full width at half-maximum (fwhm) and then compared the fwhm values for the two detected polarizations. For the rings formed on the carbon and gold substrates, the fwhm of the intensity line sections were significantly larger for directions

parallel compared to perpendicular to the polarization of the detected scattered light, as illustrated in Figure 3. In the parallel case, the average fwhm was 1040 and 1100 nm for carbon and gold, respectively, while in the perpendicular case, the average fwhm was 590 and 560 nm. However, for the ring formed on the glass substrate, the fwhm was independent of the detected polarization direction (610 and 540 nm for parallel and perpendicular, respectively). To compare these fwhm values to the optical resolution of the dark-field scattering microscope, we determined the fwhm from scattering images of single gold NPs placed on a glass coverslip. Glass was chosen as the substrate because it did not alter the image of the plasmon scattering collected for the NP ring. We measured dark-field scattering images for three different average sizes of NPs: 76, 88, and 155 nm (Figure S3 in the Supporting Information). The average fwhm of these NPs were 380, 450, and 490 nm, respectively, which demonstrate that the fwhm values were a convolution between the NP size and the microscope resolution. Because the NP rings were usually several NPs wide, corresponding to a ring thickness of approximately 100−200 nm, as shown in Figure 1, it is most appropriate to compare the fwhm of the ring and the 155 nm NPs. This comparison confirms that the intensity line sections of the ring taken in the direction parallel to the detected light polarization were significantly broadened for the carbon and gold substrates, while the intensity line sections for the perpendicular direction were mostly governed by the optical resolution.

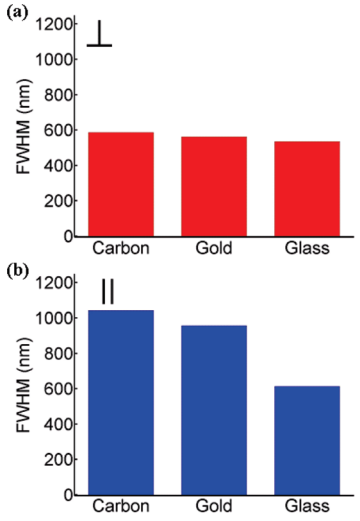

Figure 3. Full width at half-maximum (fwhm) of the intensity line sections from dark-field scattering images of self-assembled gold NP rings on carbon, gold, and glass substrates. The fwhm values were collected from the intensity line sections of ring segments which were perpendicular (a) and parallel (b) to the polarization direction of the scattered light.

The observed optical effect is assigned to the interaction of the surface plasmon resonances of the NP ring with the substrate and, in particular, the polarization component of the plasmon modes that was perpendicular to the image plane. This was confirmed by exciting the ring plasmon modes with s- and p-polarized light separately, which was achieved by placing a polarizer and a wedge in the excitation beam path.[53] By using such a combination in a reflected light dark-field microscope, which employed a large numerical aperture for excitation, and varying their orientations, s-polarized incident light was almost purely polarized "in-plane", while p-polarized excitation contained polarization components that were both parallel and perpendicular ("out-of-plane") with respect to the sample plane, where the perpendicular one dominated. Dark-field scattering images of the NP ring on the carbon and glass substrates excited with s- and p-polarized light are shown in Figure 4. For the ring supported by the carbon film, the same splitting into offset rings along the direction of the detected light polarization was observed when the image was recorded

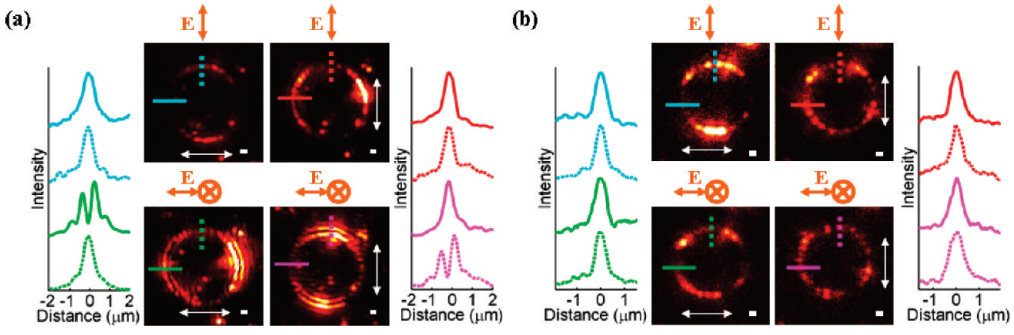

Figure 4. Dark-field scattering images of self-assembled gold NP rings on carbon (a) and glass (b) substrates for different excitation polarizations. The top row shows images for excitation with light polarized in the sample plane (s-polarized), while the bottom row contains images excited with a mixture of in-plane and out-of-plane polarized light (p-polarized). For the latter, the out-of-plane polarization component dominates. Each pair of images corresponds to the two orthogonal scattered light polarizations as indicated by the white arrows. All scale bars correspond to 1 μm. The images were corrected for background scattering, and the intensity scale ranges from 0 to 120 kHz for both carbon and glass. Intensity line sections of the ring segments that are indicated by the blue and red lines are shown to the right and left of the corresponding dark-field scattering images. The rings are the same as those shown in Figure 2. The intensity line sections were normalized and offset for better comparison.

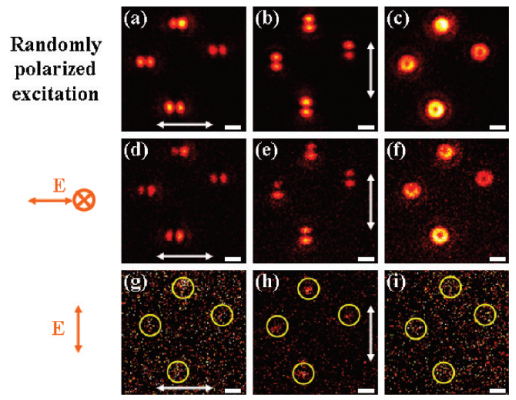

Figure 5. Dark-field scattering images of individual NPs supported by a carbon substrate for different excitation polarizations: randomly (top), p-polarized (middle), s-polarized (bottom). (a,b,d,e,g,h) Images taken with a polarizing beam splitter in the detection path; (c,f,i) images acquired without the beam splitter and only one detector. All scale bars correspond to 1 μm. The images were corrected for background scattering, and the intensity scale ranges from 0 to 900 kHz for randomly, 0 to 120 kHz for p-polarized, and 0 to 20 kHz for s-polarized excitation. Note that the wedge in the excitation path blocks out a significant portion of the light, reducing the scattering intensity. All dark-field images were taken from the same sample of 88 nm gold NPs, and the circles in the bottom row indicate the positions of the single NPs, which were too weak to be observed.

with p-polarized excitation, as illustrated in the bottom row of Figure 4a. In contrast, the splitting was clearly absent in the dark-field scattering images for excitation with s-polarized light, as shown in the top row of Figure 4a. These results and comparison to the images in Figure 2a recorded with randomly polarized excitation suggest that it was primarily the surface plasmon oscillation orientated perpendicular to the sample plane that interacted strongly with the substrate. As expected from Figure 2c, when the NP ring was supported by a glass substrate, s- and p-polarized excitation gave the same results as no noticeable splitting into offset rings is seen in any of the dark-field scattering images shown in Figure 4b.

The stronger interaction for p-polarized excitation is consistent with previous studies of individual plasmonic NPs on metallic and dielectric substrates, which furthermore found that the distance-dependent near-field coupling between the film and NP plasmons causes the individual NPs to appear as doughnuts in the optical scattering images.[25,26,29] To test if the substrates we used in this study have the same effect on the plasmon scattering images of individual NPs and what role the polarization of the incident and detected light plays, we recorded single particle scattering images of 88 nm gold NPs supported on carbon, gold, and glass substrates. Larger 88 nm NPs were used instead of the 40 nm NPs that made up the ring because the larger scattering cross section of the 88 nm NPs allowed for better contrast without changing the underlying mechanism. As expected, individual NPs on a glass substrate had a two-dimensional Gaussian intensity profile in their dark-field scattering images independent of the detected polarization (Figure S4 in the Supporting Information). However, the results for the NPs on the carbon substrate were very different, as illustrated in Figure 5, for different excitation conditions: randomly polarized (5a–c), p-polarized (5d–f), and s-polarized (5g–i). The dark-field scattering images of individual NPs were similarly affected compared to the NP ring when the surface plasmons were excited by randomly and p-polarized excitation light, which both led to a splitting of the single NP image into two lobes along the direction of the scattered light polarization (see images a, b, d, and e in Figure 5). When the individual 88 nm NPs were excited by s-polarized excitation light instead, the splitting was absent, but the scattering intensity of the NPs decreased significantly. Note the difference in intensities for the images in the middle (120 kHz full scale) and bottom (20 kHz full scale) rows of Figure 5. In agreement with previous work,[25,26,29] after removing the polarizing beam splitter and recording only one dark-field scattering image by integrating the intensity for all detected polarizations, the individual 88 nm NPs appeared as doughnuts for randomly and p-polarized excitation light (see images c and f in Figure 5). Again, when the NPs were excited by s-polarized light, no doughnut-shaped features and only a decrease in the plasmon scattering intensity was observed (see image i). The gold substrate gave the same results as those discussed for carbon (not shown). The similarity in the coupling strength for carbon and gold is further evident from the scattering spectra in Figure S5 in the Supporting Information, which show a comparable red shift of the surface plasmon resonance for the carbon and gold relative to the glass substrate.

The appearance of the doughnut-shaped features in the single NP scattering images can be explained by the induced image charge model,[17,19,25–27,29,36,37] which predicts that in-plane and out-of-plane polarized excitation results in destructive and constructive interference, respectively. Figure S6 of the Supporting Information shows a schematic description of this model for a single plasmonic NP located above a substrate. Interaction between the charge distribution created by the excitation of a plasmon oscillation in the NP with the electrons in the substrate induces an image charge distribution. Out-of-plane excitation (Figure S6a) creates an image charge dipole that is in phase with the oscillation of the NP plasmon, resulting in constructive interference. The result is the appearance of a doughnut-shaped signal in the dark-field scattering image for an individual NP, as seen in Figure 5f.[25,26,29,39,40] Note that by using an objective with a large numerical aperture in these studies it is possible to collect light with out-of-plane polarization. When a polarizing beam splitter is placed in the detection path (Figure 5d,e), the in-plane projections of the scattered light for the two

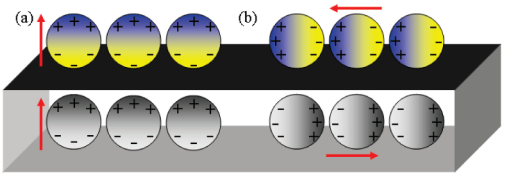

Figure 6. Schematic of the induced image charge model for a chain of three NPs located above a polarizable substrate. The three NPs represent a small segment of the ring. For out-of-plane polarized excitation light (a), the dipoles of the individual NPs are all aligned parallel to each other, forming a bright antibonding mode, and induce image dipoles having the same direction, leading to constructive interaction. For in-plane polarized excitation light (b), the dipoles of the individual NPs are again all aligned parallel to each other, forming a bright bonding mode. The induced image charges are now oscillating out of phase though, therefore canceling the collective response of the NPs. It should be noted that this picture only considers dipole plasmon modes and therefore represents only a simplified model.

orthogonal polarization components are selected. This causes the dumbbell-shaped patterns that look like a splitting of the image along the direction of the detected light polarization. On the other hand, for in-plane excitation (Figure S6b), the NP dipole and the induced image dipole are out of phase with each other, which leads to destructive interference and a strongly reduced far-field scattering intensity, as illustrated in Figure 5i. The described image charge model can also be interpreted as the hybridization of the localized surface plasmon resonance of the NP with its image charge. In fact, the model in Figure S6 (Supporting Information) resembles the case of a NP dimer.[21,47]

This induced image charge model can also be qualitatively used to explain the interactions of collective plasmon modes of the NP ring with the substrate. Figure 6 shows a schematic description of this model applied to a short chain of NPs located above a polarizable substrate. The three NPs represent a small ring segment and illustrate plasmon coupling between the NPs in the ring. Interaction between the charge distribution created by the excitation of the collective plasmon oscillation in the NPs with the electrons in the substrate induces an image charge distribution. Out-of-plane excitation (Figure 6a) creates an image charge distribution that is in phase with the plasmon oscillation of the NPs, resulting in constructive interference. In contrast, in-plane excitation (Figure 6b) creates an image charge distribution that is out of phase with the plasmon oscillation of the NPs, resulting in destructive interference. This constructive and destructive interference between the coupled plasmon modes of the NPs and the substrate image charges results in the appearance of the offset rings and the reduced scattering intensity observed in the dark-field scattering images of the NP ring shown for out-of-plane and in-plane polarized excitation, respectively. It should be noted that Figure 6 represents a simplification because only dipolar interactions are considered. In addition, only the optically active hybridized modes are shown in each case (a, antibonding; b, bonding). The collective plasmon response of the NP ring is, however, more complex because multipolar plasmon interactions become important for the short interparticle distances in the NP ring.

Because excitation of surface plasmon polaritons of the thin film by evanescent coupling of the NP to the substrate is relatively weak for dark-field illumination,[25] the collected far-field signal was dominated by scattering of the incident field by NP surface plasmons that were hybridized with induced charges situated at the surface of the substrate. The surface charge distribution due to the induced polarization is related to the localized surface plasmons of the NP by $q_{lm}^{image} = (-1)^{l+m}(1 - \varepsilon_s)/(1 + \varepsilon_s)q_{lm}$, where q_{lm} and q_{lm}^{image} are the multipolar modes of the NP and the induced image charge within the substrate, respectively;[17] ε_s is the substrate permittivity, l is the order of the plasmon mode, and m is the azimuthal index denoting out-of-plane ($m = 0$) and in-plane ($m = 1$) polarization. For a gold film, the large negative real part of its dielectric function[60] is responsible for dispersive multipolar image modes with relative magnitudes larger than the surface plasmons of the NP. These image charge oscillations can couple in or out of phase with the NP surface plasmons, leading to constructive and destructive interference in the far-field.

For dielectrics such as glass with little or no conductance, the induced dipole moment is less than that of the NP surface plasmon and oscillates completely in phase or 180° out of phase for excitation with polarization perpendicular or parallel to the substrate, respectively. However, for glass with a low permittivity of $\varepsilon_s = 2.25$, the coupling between the NP surface plasmon modes and the induced image charges is so weak that the resulting cumulative dipole moment is not very different from the response of an isolated NP.

The amorphous carbon film of the TEM substrate had a very similar influence compared to metallic gold on the scattering pattern and spectra of individual gold NPs. Carbon is indeed dispersive for the visible part of the spectrum much like gold and should therefore effectively couple to the surface plasmon of a NP for certain frequencies. Its relative absorption is, however, much weaker than that of gold. For the wavelengths most relevant for the dark-field scattering images (450−700 nm), the reported values for the real part of the permittivity of amorphous carbon span a range from 4 to 6.[61−64] These values are all larger than the permittivity of glass, consistent with the explanation of the experimental data by the image charge model. In contrast to glass, the increased broadening in the single particle scattering spectra of 88 nm gold NPs on carbon (Figure S5) furthermore indicates that the imaginary part of the permittivity for carbon (~2.5−4) also needs to be considered in the interaction between the plasmonic NPs and the induced image multipoles.

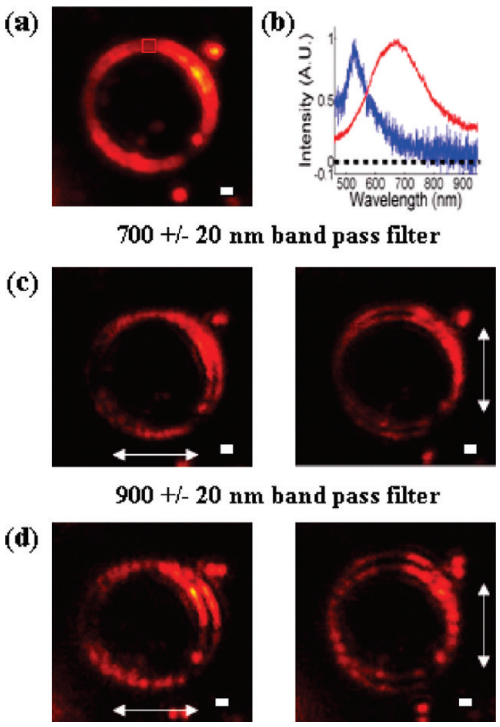

Figure 7. Dark-field scattering image (a) and spectrum (b, red line) of the same NP ring supported by a carbon substrate as shown in Figures 1 and 2. The image was taken without the polarizing beam splitter in the detection path. The red square indicates the position where the scattering spectrum was taken. The blue line in (b) shows the plasmon scattering spectrum of a single 40 nm gold NP, from which the rings were made. (c,d) Dark-field scattering images of the same ring taken with a 700 ± 20 nm band-pass filter for two orthogonal detected light polarizations as indicated by the white arrows. (e,f) Dark-field scattering images acquired with a 900 ± 20 nm band-pass filter. The scale bars correspond to 1 μm. All images were corrected for background and are displayed using the same intensity scale, which ranges from 0 to 120 kHz. The excitation light was randomly polarized for all images.

Because the carbon films used here were only 20 nm thin according to the manufacturer and a direct comparison with literature values is difficult because the permittivity has been found to vary strongly with thickness and preparation method as well as crystallinity,[62] it is difficult to draw further quantitative conclusions. Qualitatively, however, the dark-field images recorded for both carbon and gold substrates can be explained by the coupling of induced image charges with the surface plasmons of the NPs.

When the image charge model is applied to the NP rings, collective instead of localized surface plasmon modes need to be considered for the interaction with the substrate, as illustrated in Figure 6. Because of the random arrangement of the NPs within the ring and considering the optical resolution, it is unlikely that the observed effect could simply be due to a superposition of the response from all of the individual NPs that made up the ring. This conclusion is further supported by wavelength resolved dark-field imaging (Figure 7). We

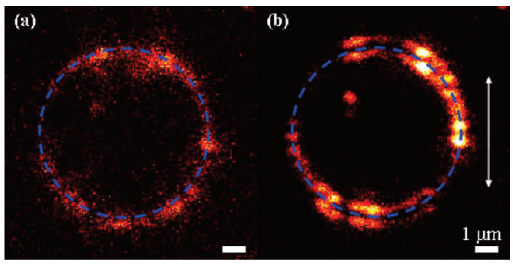

Figure 8. Dark-field scattering images of a gold NP ring on a carbon substrate recorded with (a) s-polarized and (b) p-polarized excitation light. The blue circle in both images indicates the physical location of the NP ring. The detection polarization was vertical as indicated by the arrow. Both images were corrected for background and are displayed using the same intensity scale, which ranges from 0 to 100 kHz.

have previously investigated the polarized scattering spectra of self-assembled NP rings supported on glass and observed the emergence of multipolar collective plasmon modes due to strong near-field coupling between adjacent NPs in the ring.[58] These collective plasmon resonances were mainly polarized along the ring circumference. Figure 7a shows a dark-field image of a NP ring on the carbon substrate and its spectrum (Figure 7b) collected from the area marked by the red square. For both of these measurements, the polarizing beam splitter was removed and the excitation light was randomly polarized. The spectrum of the NP ring was much broader and red-shifted from the plasmon resonance of a single constituent 40 nm gold NP, shown for comparison as the blue line in Figure 7b. The fact that the scattering spectrum of the ring extended beyond 900 nm suggests that the lowest order mode was shifted to longer wavelengths outside our experimental spectral window. Despite the different substrate, the ring spectrum in Figure 7b is consistent with our previous results.[58]

To prove that the interaction between the substrate and the collective plasmon modes of the ring and not the localized plasmon resonance of the individual NPs is responsible for the appearance of the offset rings, we collected wavelength resolved dark-field scattering images for the NP ring supported by the carbon substrate. This was achieved by placing various band-pass filters in the detection path. Figure 7c shows dark-field images recorded with a 700 nm band-pass filter for two orthogonal polarizations of the detected light and randomly polarized excitation, while Figure 7d contains the corresponding images for a 900 nm band-pass filter. The rings were clearly split again into two offset circles for these two wavelengths, which were red-shifted from the single NP response. At these red-shifted wavelengths, transverse plasmon modes must effectively couple with the substrate as ring segments aligned perpendicularly to the direction of the detected polarization appear brighter with p-polarized excitation light (see bottom of Figure 4a). It can therefore be concluded that it must be the interaction between the oscillating charges of the collective ring

modes and their induced image charges that caused the observed optical effect. We can furthermore rationalize now why the scattering intensity for the NP ring was not as strongly suppressed for s-polarized compared to p-polarized excitation (Figure 4a) as expected from the corresponding results shown for the individual gold NPs in Figure 5. The collective optical response of the NP ring contains many plasmon modes with both in-plane and out-of-plane polarization components, and a simple cancellation of opposing dipoles as is the case for single NPs is therefore not possible. These wavelength resolved dark-field scattering images furthermore illustrate that even the most red-shifted coupled plasmon modes of the ring possess transverse polarization components, which were only very weak or absent in the previously published polarized scattering spectra.[58]

Interestingly, the wavelength resolved dark-field images in Figure 7 provide further evidence for the proposed image charge model by analyzing the fwhm of the intensity line sections. We observed that the fwhm values were dependent on the wavelength of the detected scattered light. The fwhm values of the line sections analyzed parallel to the scattered light polarization were significantly different for the images taken with the 900 $\pm$ 20 nm band-pass filter compared to the 700 $\pm$ 20 nm band-pass filter: the average fwhm value of the line section from the image taken with the 900 $\pm$ 20 nm band-pass filter was 1360 nm, while the average fwhm value of the line section from the image taken with the 700 $\pm$ 20 nm band-pass filter was 1050 nm. This difference is consistent with an interference between the collective ring modes and the induced image charges in the substrate. The spacing of the interference fringes depends on the wavelength of the interfering waves. Longer wavelengths result in larger spacings between the fringes as observed here.

The question arises as to where the NPs of the ring actually were in the optical images that were split into offset circles. We found that the physical position of the ring was in the middle of the two offset circles, which in turn means that the offset circles in the scattering images were displaced from the NP ring's actual location. Figure 8 shows two images of the same NP ring on a carbon substrate, which were acquired with different incident polarizations in order to produce images that intentionally either displayed a single ring (8a) or two offset circles (8b). In Figure 8a, the physical location of the NP ring must coincide with the optical signal and is indicated by the blue dashed circle. By superimposing the two images in Figure 8, taking advantage of additional reference points in the images, we can conclude that the location of the NP ring was in between the offset circles. Figure S7 in the Supporting Information further supports our conclusion about the physical location of the NP ring as the difference of two dark-field scattering images with orthogonal polarizations agrees well with simulations.

CONCLUSIONS AND PROSPECTS

We have observed strong coupling between collective plasmon modes in NP rings and the substrate which supported the self-assembled structures. In the dark-field scattering images, this interaction was seen as a splitting of the ring image into two offset circles along the direction of the detected light polarization. By isolating different polarization components of the excitation light, we showed that the coupling responsible for this effect was strongest for polarization perpendicular to the substrate. We interpret the splitting into offset rings as the coupling between collective plasmon modes of the ring and induced images charges in the substrate as verified by single particle measurements and wavelength resolved dark-field imaging. The strength of this coupling was dependent on the nature of the substrate as no effect was seen for NP rings on a low permittivity substrate such a glass. The experimental results for the optical response of individual and assembled gold NPs on the carbon compared to the gold film suggest a similar interaction strength, which is important to consider when using carbon-coated TEM grids as NP substrates. Finally, our results show how it is possible to spatially modulate scattering from plasmonic nanostructures. Changing the permittivity of the substrate through external control with electrical or optical signals could tune the optical response of supported plasmonic structures by turning on and off the coupling with induced image charges. The result for a NP assembly as reported here would be a plasmonic light modulator similar to an acousto-optic modulator used in optics to deflect the beam path of laser light by a few degrees, but operating on the scale of a few micrometers. One can furthermore envision using the effect discussed in this work to sense changes in the dielectric properties of the supporting substrate.

METHODS

Gold NPs (40 nm) with a polystyrene surface coating (M_w = 10 000 g/mol) were prepared and stored in dichloromethane following the procedure described elsewhere.[59] Self-assembled rings were prepared by allowing a drop of the solution containing the functionalized NPs to dry on different substrates. NP rings of various sizes ranging from about 1 to 10 μm in diameter were formed at the interface between the organic solvent and water droplets that condensed from the air due to dichloromethane evaporation. We used glass coverslips as substrates for the NP rings (Fisher 12-541-B), ~15 nm thin gold patterns deposited on glass coverslips, and ~20 nm

thin carbon films on top of standard TEM copper grids (Ted Pella CF300-Cu-50). The gold patterns were formed using an indexed TEM grid (Ted Pella 79021C) and an electron beam evaporator (Telemark), which also allowed us to locate the same structures on the glass and gold substrates by optical microscopy and scanning electron microscopy (FEI Quanta ESEM2 operated at 25 kV in wet mode).[58,65,66] The samples deposited on TEM grids were characterized using a transmission electron microscope (JEOL 2010) operated at 120 kV.

Dark-field excitation was performed in a reflected light geometry using an inverted microscope (Zeiss Axiovert 200) with a halogen lamp as the excitation source. Dark-field contrast was achieved using incident excitation light with a numerical aperture larger than that for the collected backscattered light. The polarization of the excitation light was selected using a combination of a wedge and a polarizer.[52] To allow for coarse and fine adjustments of the sample position, a custom-designed holder was attached to a manual translational stage and mounted on an *xyz* piezo scanning stage (Physik Instrumente P-517.3CL), which was connected to a surface probe microscope controller (RHK Technology SPM 1000). Scattered light was collected with a Zeiss Epiplan 100×/0.75 objective and, after passing first through a 50 μm pinhole located at the first microscope image plane and then a polarizing beam splitter, was focused onto two avalanche photodiode detectors (Perkin-Elmer SPCM-AQR-15). Using an intermediate 2.5× lens gave a total magnification of 250× at the detectors. Dark-field scattering images were collected point by point with the scanning stage. Optical density and band-pass filters were used in the detection path to prevent saturating the detectors and to collect images for specific wavelength intervals of the scattered light, respectively. Scattering spectra were acquired by redirecting the light to the entrance of a spectrometer (Princeton Instruments Acton SP2150i) connected to a CCD camera (Princeton Instruments PIXIS 400BR). A Zeiss Epiplan-Neofluar 50×/0.8 objective was used to measure spectra and wavelength resolved images because it has a better transmission efficiency and chromatic correction for wavelengths longer than 700 nm compared to the 100× Epiplan objective. The spectra were corrected for background and dark counts by measuring spectra at regions with no NPs present and with the lamp off, respectively. In addition, correction for the spectral response of the lamp and other optical components was carried out by collecting the spectrum of a white light reflectivity standard (Labsphere SRS-99-010).

Acknowledgment. S.L. thanks the Robert A. Welch Foundation (Grant C-1664), NSF (CHE-0955286), the ACS Petroleum Research Fund (50191-DNI6), and 3M for a Nontenured Faculty Grant. E.R.Z. acknowledges financial support by NSF (DMR-0547399) and the Robert A. Welch Foundation (C-1703). P.S. acknowledges support from the Royal Thai Government, and L.S.S. thanks the NSF IGERT Nanophotonics fellowship program. W.S.C. acknowledges support from the Richard E. Smalley Institute for a Peter and Ruth Nicholas fellowship. We thank Avishek Saha for help with TEM measurements.

Supporting Information Available: SEM images of NP rings on gold and glass substrates, a microscope focus dependence of the dark-field scattering images, the optical resolution for dark-field scattering of single gold NPs with different sizes, dark-field scattering images of 88 nm NPs on carbon and glass substrates, dark-field scattering spectra of 88 nm NPs on carbon, gold, and glass substrates, schematic of the induced image charge model for a single NP on a polarizable substrate, and an analysis for the physical location of the NP ring in the dark-field image. This material is available free of charge *via* the Internet at http://pubs.acs.org.

REFERENCES AND NOTES

1. Kelly, K. L.; Coronado, E.; Zhao, L. L.; Schatz, G. C. The Optical Properties of Metal Nanoparticles: The Influence of Size, Shape, and Dielectric Environment. *J. Phys. Chem. B* **2003**, *107*, 668–677.
2. Lal, S.; Link, S.; Halas, N. J. Nano-Optics from Sensing to Waveguiding. *Nat. Photonics* **2007**, *1*, 641–648.
3. Noguez, C. Surface Plasmons on Metal Nanoparticles: The Influence of Shape and Physical Environment. *J. Phys. Chem. C* **2007**, *111*, 3806–3819.
4. Jain, P. K.; Lee, K. S.; El-Sayed, I. H.; El-Sayed, M. A. Calculated Absorption and Scattering Properties of Gold Nanoparticles of Different Size, Shape, and Composition: Applications in Biological Imaging and Biomedicine. *J. Phys. Chem. B* **2006**, *110*, 7238–7248.
5. Miller, M. M.; Lazarides, A. A. Sensitivity of Metal Nanoparticle Surface Plasmon Resonance to the Dielectric Environment. *J. Phys. Chem. B* **2005**, *109*, 21556–21565.
6. Landes, C. F.; Link, S.; Mohamed, M. B.; Nikoobakht, B.; El-Sayed, M. A. Some Properties of Spherical and Rod-Shaped Semiconductor and Metal Nanocrystals. *Pure Appl. Chem.* **2002**, *74*, 1675–1692.
7. Willets, K. A.; Van Duyne, R. P. Localized Surface Plasmon Resonance Spectroscopy and Sensing. *Annu. Rev. Phys. Chem.* **2007**, *58*, 267–297.
8. Raschke, G.; Kowarik, S.; Franzl, T.; Sönnichsen, C.; Klar, T. A.; Feldmann, J.; Nichtl, A.; Kürzinger, K. Biomolecular Recognition Based on Single Gold Nanoparticle Light Scattering. *Nano Lett.* **2003**, *3*, 935–938.
9. Sherry, L. J.; Chang, S.-H.; Schatz, G. C.; Van Duyne, R. P.; Wiley, B. J.; Xia, Y. Localized Surface Plasmon Resonance Spectroscopy of Single Silver Nanocubes. *Nano Lett.* **2005**, *5*, 2034–2038.
10. Nehl, C. L.; Liao, H.; Hafner, J. H. Optical Properties of Star-Shaped Gold Nanoparticles. *Nano Lett.* **2006**, *6*, 683–688.
11. Chen, H. J.; Kou, X. S.; Yang, Z.; Ni, W. H.; Wang, J. F. Shape- and Size-Dependent Refractive Index Sensitivity of Gold Nanoparticles. *Langmuir* **2008**, *24*, 5233–5237.
12. Malinsky, M. D.; Kelly, K. L.; Schatz, G. C.; Van Duyne, R. P. Nanosphere Lithography: Effect of Substrate on the Localized Surface Plasmon Resonance Spectrum of Silver Nanoparticles. *J. Phys. Chem. B* **2001**, *105*, 2343–2350.
13. Novo, C.; Funston, A. M.; Pastoriza-Santos, I.; Liz-Marzan, L. M.; Mulvaney, P. Influence of the Medium Refractive Index on the Optical Properties of Single Gold Triangular Prisms on a Substrate. *J. Phys. Chem. C* **2008**, *112*, 3–7.
14. Sherry, L. J.; Jin, R.; Mirkin, C. A.; Schatz, G. C.; Van Duyne, R. P. Localized Surface Plasmon Resonance Spectroscopy of Single Silver Triangular Nanoprisms. *Nano Lett.* **2006**, *6*, 2060–2065.
15. Murray, W. A.; Auguie, B.; Barnes, W. L. Sensitivity of Localized Surface Plasmon Resonances to Bulk and Local Changes in the Optical Environment. *J. Phys. Chem. C* **2009**, *113*, 5120–5125.
16. Chance, R. R.; Prock, A.; Silbey, R. Frequency Shifts of an Electric-Dipole Transition near a Partially Reflecting Surface. *Phys. Rev. A* **1975**, *12*, 1448–1452.
17. Jackson, J. D. *Classical Electrodynamics*, 3rd ed.; John Wiley & Sons, Inc.: Toronto, 1999.
18. Bobbert, P. A.; Vlieger, J. Light Scattering by a Sphere on a Substrate. *Physica A* **1986**, *137A*, 209–242.
19. Wind, M. M.; Vlieger, J.; Bedeaux, D. The Polarizability of a Truncated Sphere on a Substrate I. *Physica A* **1987**, *141*, 33–57.
20. Kim, J. H.; Ehrman, S. H.; Mulholland, G. W.; Germer, T. A. Polarized Light Scattering by Dielectric and Metallic Spheres on Silicon Wafers. *Appl. Opt.* **2002**, *41*, 5405–5412.
21. Nordlander, P.; Prodan, E. Plasmon Hybridization in Nanoparticles near Metallic Surfaces. *Nano Lett.* **2004**, *4*, 2209–2213.
22. Nordlander, P.; Le, F. Plasmonic Structure and Electromagnetic Field Enhancements in the Metallic Nanoparticle-Film System. *Appl. Phys. B: Laser Opt.* **2006**, *84*, 35–41.
23. Lévêque, G.; Martin, O. J. F. Optical Interactions in a Plasmonic Particle Coupled to a Metallic Film. *Opt. Exp.* **2006**, *14*, 9971–9981.
24. Le, F.; Lwin, N. Z.; Steele, J. M.; Käll, M.; Halas, N. J.; Nordlander, P. Plasmons in the Metallic Nanoparticle−Film System as a Tunable Impurity Problem. *Nano Lett.* **2005**, *5*, 2009–2013.
25. Mock, J. J.; Hill, R. T.; Degiron, A.; Zauscher, S.; Chilkoti, A.; Smith, D. R. Distance-Dependent Plasmon Resonant

Coupling between a Gold Nanoparticle and Gold Film. *Nano Lett.* **2008**, *8*, 2245–2252.
26. Hu, M.; Ghoshal, A.; Marquez, M.; Kik, P. G. Single Particle Spectroscopy Study of Metal-Film-Induced Tuning of Silver Nanoparticle Plasmon Resonances. *J. Phys. Chem. C* **2010**, *114*, 7509–7514.
27. Okamoto, T.; Yamaguchi, I. Optical Absorption Study of the Surface Plasmon Resonance in Gold Nanoparticles Immobilized onto a Gold Substrate by Self-Assembly Technique. *J. Phys. Chem. B* **2003**, *107*, 10321–10324.
28. Abe, S.; Kajikawa, K. Linear and Nonlinear Optical Properties of Gold Nanospheres Immobilized on a Metallic Surface. *Phys. Rev. B* **2006**, *74*, No. 035416.
29. Chen, S. Y.; Mock, J. J.; Hill, R. T.; Chilkoti, A.; Smith, D. R.; Lazarides, A. A. Gold Nanoparticles on Polarizable Surfaces as Raman Scattering Antennas. *ACS Nano* **2010**, *4*, 6535–6546.
30. Sisco, P. N.; Murphy, C. J. Surface-Coverage Dependence of Surface-Enhanced Raman Scattering from Gold Nanocubes of Self-Assembled Monolayers of Analyte. *J. Phys. Chem. A* **2009**, *113*, 3973–3978.
31. Park, W.-H.; Kim, Z. H. Charge Transfer Enhancement in the SERS of a Single Molecule. *Nano Lett.* **2010**, *10*, 4040–4048.
32. Hill, R. T.; Mock, J. J.; Urzhumov, Y.; Sebba, D. S.; Oldenburg, S. J.; Chen, S.-Y.; Lazarides, D. A.; Chilkoti, A.; Smith, D. R. Leveraging Nanoscale Plasmonic Modes To Achieve Reproducible Enhancement of Light. *Nano Lett.* **2010**, *10*, 4150–4154.
33. Eah, S.-K.; Jaeger, H. M.; Scherer, N. F.; Wiederrecht, G. P.; Lin, X.-M. Scattered Light Interference from a Single Metal Nanoparticle and Its Mirror Image. *J. Phys. Chem. B* **2005**, *109*, 11858–11861.
34. Ringe, E.; McMahon, J. M.; Sohn, K.; Cobley, C.; Xia, Y.; Huang, J.; Schatz, G. C.; Marks, L. D.; Van Duyne, R. P. Unraveling the Effects of Size, Composition, and Substrate on the Localized Surface Plasmon Resonance Frequencies of Gold and Silver Nanocubes: A Systematic Single-Particle Approach. *J. Phys. Chem. C* **2010**, *114*, 12511–12516.
35. Knight, M. W.; Wu, Y.; Lassiter, J. B.; Nordlander, P.; Halas, N. J. Substrates Matter: Influence of an Adjacent Dielectric on an Individual Plasmonic Nanoparticle. *Nano Lett.* **2009**, *9*, 2188–2192.
36. Pinchuk, A.; Hilger, A.; von Plessen, G.; Kreibig, U. Substrate Effect on the Optical Response of Silver Nanoparticles. *Nanotechnology* **2004**, *15*, 1890–1896.
37. Wu, Y.; Nordlander, P. Finite-Difference Time-Domain Modeling of the Optical Properties of Nanoparticles near Dielectric Substrates. *J. Phys. Chem. C* **2010**, *114*, 7302–7307.
38. You, Y.-M.; Du, C.-L.; Ma, Y.; Kasim, J.; Yu, T.; Shen, Z.-X. Effect of Near-Field Coupling on Far-Field Inelastic Scattering Imaging of Gold Nanoparticles. *Nanotechnology* **2008**, *19*, 395705.
39. Bartko, A. P.; Dickson, R. M. Three-Dimensional Orientations of Polymer-Bound Single Molecules. *J. Phys. Chem. B* **1999**, *103*, 3053–3056.
40. Moerland, R. J.; Taminiau, T. H.; Novotny, L.; van Hulst, N. F.; Kuipers, L. Reversible Polarization Control of Single Photon Emission. *Nano Lett.* **2008**, *8*, 606–610.
41. Patra, D.; Gregor, I.; Enderlein, J. Image Analysis of Defocused Single-Molecule Images for Three-Dimensional Molecule Orientation Studies. *J. Phys. Chem. A* **2004**, *108*, 6836–6841.
42. Curto, A. G.; Volpe, G.; Taminiau, T. H.; Kreuzer, M. P.; Quidant, R.; van Hulst, N. F. Unidirectional Emission of a Quantum Dot Coupled to a Nanoantenna. *Science* **2010**, *329*, 930–933.
43. Kühn, S.; Mori, G.; Agio, M.; Sandoghdar, V. Modification of Single Molecule Fluorescence Close to a Nanostructure: Radiation Pattern, Spontaneous Emission and Quenching. *Mol. Phys.* **2008**, *106*, 893–908.
44. Taminiau, T. H.; Stefani, F. D.; Segerink, F. B.; van Hulst, N. F. Optical Antennas Direct Single-Molecule Emission. *Nat. Photonics* **2008**, *2*, 234–237.
45. Kosako, T.; Koadoya, Y.; Hofman, H. F. Directional Control of Light by a Nano-Optical Yagi-Uda Antenna. *Nat. Photonics* **2010**, *4*, 312–315.
46. Chen, H. J.; Sun, Z. H.; Ni, W. H.; Woo, K. C.; Lin, H. Q.; Sun, L. D.; Yan, C. H.; Wang, J. F. Plasmon Coupling in Clusters Composed of Two-Dimensionally Ordered Gold Nanocubes. *Small* **2009**, *5*, 2111–2119.
47. Gozhenko, V. V.; Grechko, L. G.; Whites, K. W. Electrodynamics of Spatial Clusters of Spheres: Substrate Effects. *Phys. Rev. B* **2003**, *68*, No. 125422.
48. Vernon, K. C.; Funston, A. M.; Novo, C.; Gomez, D. E.; Mulvaney, P.; Davis, T. J. Influence of Particle−Substrate Interaction on Localized Plasmon Resonances. *Nano Lett.* **2010**, *10*, 2080–2086.
49. Xu, G.; Chen, Y.; Tazawa, M.; Jin, P. Surface Plasmon Resonance of Silver Nanoparticles on Vanadium Dioxide. *J. Phys. Chem. B* **2006**, *110*, 2051–2056.
50. Su, K. H.; Wei, Q. H.; Zhang, X.; Mock, J. J.; Smith, D. R.; Schultz, S. Interparticle Coupling Effects on Plasmon Resonances of Nanogold Particles. *Nano Lett.* **2003**, *3*, 1087–1090.
51. Romero, I.; Aizpurua, J.; Bryant, G. W.; Garcia de Abajo, F. J. Plasmons in Nearly Touching Metallic Nanoparticles: Singular Response in the Limit of Touching Dimers. *Opt. Express* **2006**, *14*, 9988–9999.
52. Tamaru, H.; Kuwata, H.; Miyazaki, H. T.; Miyano, K. Resonant Light Scattering from Individual Ag Nanoparticles and Particle Pairs. *Appl. Phys. Lett.* **2002**, *80*, 1826–1828.
53. Lassiter, J. B.; Aizpurua, J.; Hernandez, L. I.; Brandl, D. W.; Romero, I.; Lal, S.; Hafner, J. H.; Nordlander, P.; Halas, N. J. Close Encounters between Two Nanoshells. *Nano Lett.* **2008**, *8*, 1212–1218.
54. Jain, P. K.; Huang, W.; El-Sayed, M. A. On the Universal Scaling Behavior of the Distance Decay of Plasmon Coupling in Metal Nanoparticle Pairs: A Plasmon Ruler Equation. *Nano Lett.* **2007**, *7*, 2080–2088.
55. Chen, J. I. L.; Chen, Y.; Ginger, D. S. Plasmonic Nanoparticle Dimers for Optical Sensing of DNA in Complex Media. *J. Am. Chem. Soc.* **2010**, *132*, 9600–9601.
56. Chandra, M.; Dowgiallo, A.-M.; Knappenberger, K. L., Jr. Controlled Plasmon Resonance Properties of Hollow Gold Nanosphere Aggregates. *J. Am. Chem. Soc.* **2010**, *132*, 15782–15789.
57. Slaughter, L. S.; Wu, Y.; Willingham, B. A.; Nordlander, P.; Link, S. Effects of Symmetry Breaking and Conductive Contact on the Plasmon Coupling in Gold Nanorod Dimers. *ACS Nano* **2010**, *4*, 4657–4666.
58. Chang, W. S.; Slaughter, L. S.; Khanal, B. P.; Manna, P.; Zubarev, E. R.; Link, S. One-Dimensional Coupling of Gold Nanoparticle Plasmons in Self-Assembled Ring Superstructures. *Nano Lett.* **2009**, *9*, 1152–1157.
59. Khanal, B. P.; Zubarev, E. R. Rings of Nanorods. *Angew. Chem., Int. Ed.* **2007**, *46*, 2195–2198.
60. Johnson, P. B.; Christy, R. W. Optical Constants of the Noble Metals. *Phys. Rev. B* **1972**, *6*, 4370–4379.
61. Berlind, T.; Furlan, A.; Czigany, Z.; Neidhardt, J.; Hultman, L.; Arwin, H. Spectroscopic Ellipsometry Characterization of Amorphous Carbon and Amorphous, Graphitic and Fullerene-like Carbon Nitride Thin Films. *Thin Solid Films* **2009**, *517*, 6652–6658.
62. Gioti, M.; Logothetidis, S. Dielectric Function, Electronic Properties and Optical Constants of Amorphous Carbon and Carbon Nitride Films. *Diamond Relat. Mater.* **2003**, *12*, 957–962.
63. Parker, W. G.; Watson, T. J.; Sambles, J. R. The Optical Dielectric Function of Amorphous Carbon Films. *Thin Solid Films* **1996**, *279*, 162–165.
64. Logothetidis, S. Optical and Electronic Properties of Amorphous Carbon Materials. *Diamond Relat. Mater.* **2003**, *12*, 141–150.
65. Slaughter, L. S.; Chang, W.-S.; Swanglap, P.; Tcherniak, A.; Khanal, B. P.; Zubarev, E. R.; Link, S. Single-Particle Spectroscopy of Gold Nanorods beyond the Quasi-Static Limit: Varying the Width at Constant Aspect Ratio. *J. Phys. Chem. C* **2010**, *114*, 4934–4938.
66. Tcherniak, A.; Ha, J. W.; Dominguez-Medina, S.; Slaughter, L. S.; Link, S. Probing a Century Old Prediction One Plasmonic Particle at a Time. *Nano Lett.* **2010**, *10*, 1398–1404.